nature climate change

LETTERS

https://doi.org/10.1038/s41558-018-0339-y

Polar amplification dominated by local forcing and feedbacks

Malte F. Stuecker[1,2*], Cecilia M. Bitz[3], Kyle C. Armour[3,4], Cristian Proistosescu[5], Sarah M. Kang[6], Shang-Ping Xie[7], Doyeon Kim[6], Shayne McGregor[8,9], Wenjun Zhang[10], Sen Zhao[10,11], Wenju Cai[12,13], Yue Dong[3] and Fei-Fei Jin[11]

The surface temperature response to greenhouse gas forcing displays a characteristic pattern of polar-amplified warming[1–5], particularly in the Northern Hemisphere. However, the causes of this polar amplification are still debated. Some studies highlight the importance of surface-albedo feedback[6–8], while others find larger contributions from longwave feedbacks[4,9,10], with changes in atmospheric and oceanic heat transport also thought to play a role[11–16]. Here, we determine the causes of polar amplification using climate model simulations in which CO_2 forcing is prescribed in distinct geographical regions, with the linear sum of climate responses to regional forcings replicating the response to global forcing. The degree of polar amplification depends strongly on the location of CO_2 forcing. In particular, polar amplification is found to be dominated by forcing in the polar regions, specifically through positive local lapse-rate feedback, with ice-albedo and Planck feedbacks playing subsidiary roles. Extra-polar forcing is further shown to be conducive to polar warming, but given that it induces a largely uniform warming pattern through enhanced poleward heat transport, it contributes little to polar amplification. Therefore, understanding polar amplification requires primarily a better insight into local forcing and feedbacks rather than extra-polar processes.

Polar amplification—commonly defined as the ratio of polar warming to tropical warming[4,10]—is a robust feature of climate change seen in historical observations and climate model simulations[1–5]. Accurate predictions of polar warming are critical given the fundamental role that polar ice plays in the climate system, terrestrial and marine ecosystems, and human society.

A key challenge is identifying the roles that local (that is, polar) and remote (that is, extra-polar) processes play in polar amplification within the inherently coupled climate system. Indeed, different conclusions have been reached as to which feedbacks most contribute to polar amplification and whether poleward heat transport plays a significant role[4,5,7–14,17,18]. These differences may, in part, be due to different analysis methods. For instance: using simulations with prescribed changes in sea-ice and sea-surface temperatures (SSTs), Screen et al.[7] argue that sea-ice loss is the main contributor to Arctic surface warming. In contrast, within freely evolving coupled model simulations driven by CO_2 forcing, Pithan and Mauritsen[4] diagnose the lapse-rate feedback as the leading cause of Arctic amplification, with little role for changes in poleward heat transport. Using yet another approach based on diagnostics of atmospheric re-analyses over a period that includes the effects of both internal variability and forcing, Lee et al.[13] suggest that observed Arctic amplification was driven primarily by increased downwelling radiation at the surface—perhaps arising from increased moisture intrusions into the Arctic during autumn and winter[19]—associated with anomalous planetary waves generated by convective heating in the tropics[13].

Here, we perform an idealized hierarchy of atmosphere–ocean general circulation model simulations aimed at quantifying the relative contributions of local and remote processes to polar amplification under greenhouse gas forcing (Methods). Specifically, we contrast the polar climate response to CO_2 radiative forcing applied locally[17,18,20,21] in the polar regions (POLAR; CO_2 increased over 60° S–90° S and 60° N–90° N) against a remote CO_2 radiative forcing applied in the deep tropics (TROP; CO_2 increased over 7° S–7° N). The deep tropics region is defined such that the area over which forcing is applied is approximately equal to that of the polar forcing. Additionally, we conduct simulations with CO_2 forcing applied (1) in the rest of the tropics, subtropics and midlatitudes (MLAT; CO_2 increased over 8° S–59° S and 8° N–59° N) and (2) globally (GLOBAL; CO_2 increased over 90° S–90° N) to examine the linearity of the climate response to regional forcings (that is, do the responses to forcings applied in distinct regions sum to that of CO_2 forcing applied globally?). In all cases, CO_2 concentrations are abruptly quadrupled from their pre-industrial levels, and multiple ensemble members are used to ensure that the forced signal is isolated (Methods).

This experimental setup allows us to prognostically investigate the contributions of local (that is, POLAR) and remote (that is, TROP and MLAT) forcing, feedbacks and heat transport to polar amplification in the coupled climate system (coupled simulations denoted CPL). We focus our analysis of CPL simulations on the response averaged over years 11–60 following CO_2 quadrupling—an idealized representation of the transient warming expected from

[1]Center for Climate Physics, Institute for Basic Science, Busan, Republic of Korea. [2]Pusan National University, Busan, Republic of Korea. [3]Department of Atmospheric Sciences, University of Washington, Seattle, WA, USA. [4]School of Oceanography, University of Washington, Seattle, WA, USA. [5]Joint Institute for the Study of the Atmosphere and Ocean, University of Washington, Seattle, WA, USA. [6]School of Urban and Environmental Engineering, Ulsan National Institute of Science and Technology, Ulsan, Republic of Korea. [7]Scripps Institution of Oceanography, University of California San Diego, San Diego, CA, USA. [8]School of Earth, Atmosphere and Environment, Monash University, Melbourne, Victoria, Australia. [9]ARC Centre of Excellence for Climate Extremes, Sydney, New South Wales, Australia. [10]Key Laboratory of Meteorological Disaster of Ministry of Education, College of Atmospheric Sciences, Nanjing University of Information Science and Technology, Nanjing, China. [11]Department of Atmospheric Sciences, University of Hawaii at Manoa, Honolulu, HI, USA. [12]Key Laboratory of Physical Oceanography/Institute for Advanced Ocean Studies, Ocean University of China and Qingdao National Laboratory for Marine Science and Technology, Qingdao, China. [13]Centre for Southern Hemisphere Oceans Research, CSIRO Oceans and Atmosphere, Hobart, Tasmania, Australia. *e-mail: stuecker@pusan.ac.kr

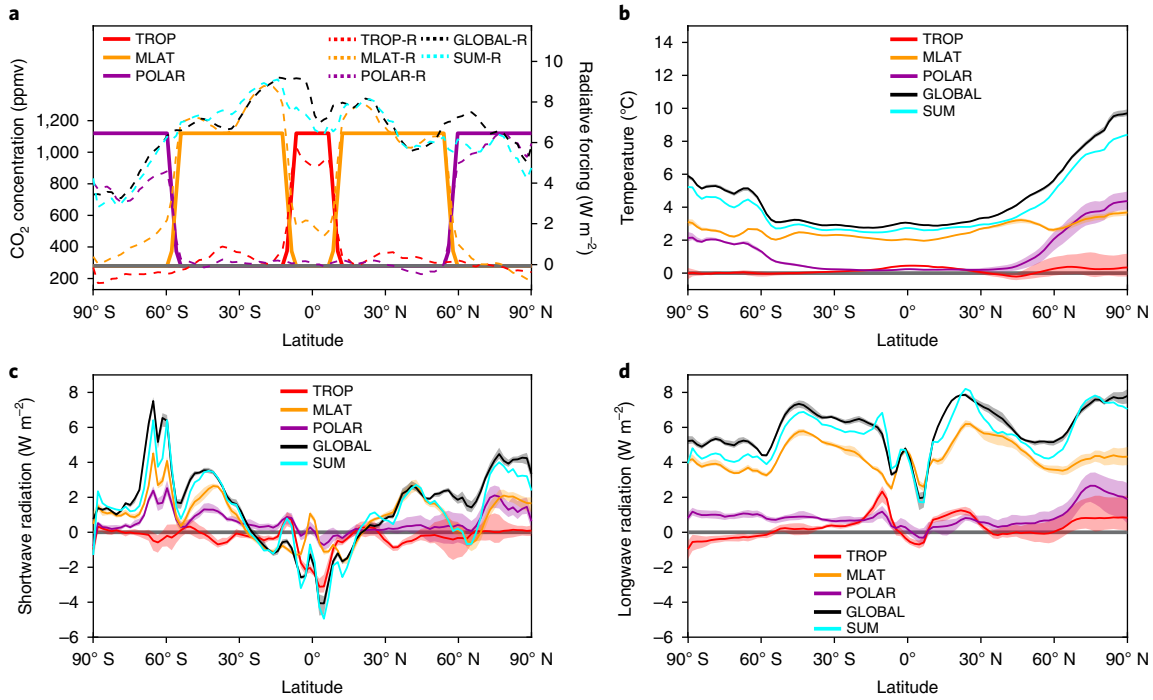

Fig. 1 | Forcing structure and climate response. a, CO_2 forcing structure for the experiments TROP (solid red), MLAT (solid orange) and POLAR (solid magenta), and radiative forcing (net TOA shortwave – net TOA longwave) from TROP-AGCM (dashed red), MLAT-AGCM (dashed orange), POLAR-AGCM (dashed magenta) and GLOBAL-AGCM (dashed black), as well as the sum (dashed cyan) from the regional experiments. **b**–**d**, Zonal mean climate responses for TROP-CPL (solid red), MLAT-CPL (solid orange), POLAR-CPL (solid magenta) and GLOBAL-CPL (solid black). Shading indicates the ensemble range. The sum for the regional experiments is indicated by solid cyan. **b**, TAS response. **c**, Shortwave feedback (absorbed TOA shortwave CPL response − shortwave radiative forcing). **d**, Longwave feedback (outgoing TOA longwave CPL response − longwave radiative forcing).

forcing sometime this coming century relative to pre-industrial conditions (Methods). To isolate the role of ocean circulation changes, we also perform simulations that are identical to CPL except for the use of a mixed-layer slab ocean model (SOM). We determine the radiative forcing of quadrupling CO_2 concentrations in each region by conducting atmospheric general circulation model (AGCM) simulations with fixed SST and sea-ice boundary conditions. The top-of-the-atmosphere (TOA) radiative imbalance in these experiments relative to an AGCM control simulation defines the effective (troposphere-adjusted) radiative forcing associated with CO_2 quadrupling (Methods). The sum of the radiative forcing in each of the regions matches that of global forcing well (Fig. 1a).

In both CPL and SOM experiments, the sum of the near-surface air temperature at 2 m reference height (TAS) responses to regional forcing approximates the response to global forcing well (Fig. 1b and Supplementary Fig. 1)—in good agreement with an earlier idealized aquaplanet study[18]. Notably, this linearity also holds for the individual TOA shortwave (Fig. 1c) and longwave (Fig. 1d) radiative responses to surface warming. These results hold over both poles, although Antarctic amplification is smaller than Arctic amplification (Fig. 1b). This spatial linearity is a key result as it suggests that polar warming in GLOBAL can be decomposed in terms of the responses to forcing in each region individually.

Due to their equivalent spatial coverage, the relative contributions of TROP and POLAR forcing to surface warming can be directly compared: both induce comparable amounts of warming within the tropics (30° S–30° N), but POLAR induces a factor of four more global mean warming and an order of magnitude more warming at the poles, consistent with previous studies of localized forcing patterns[18,22]. The largest global mean warming comes from MLAT, but this is attributable to applying the forcing over a greater area; per unit global mean forcing, POLAR induces the largest global mean warming (Table 1).

Crucially, both extra-polar forcings (MLAT and TROP) show a nearly spatially uniform pattern of surface warming with little polar amplification (Fig. 1b and Table 1). Therefore, while polar warming is influenced by tropical and midlatitude forcing, polar amplification is almost entirely due to local polar processes with little direct role for remote forcing. These results hold at equilibrium (SOM results shown in Supplementary Fig. 1), as well as in winter and summer (Supplementary Fig. 2).

Next, we consider the tropospheric temperature response to the distinct regional forcings. Polar forcing results in strong near-surface and lower-tropospheric warming at the poles for both CPL (Fig. 2c) and SOM (Supplementary Fig. 3c) experiments. Extra-polar forcing results in a more vertically uniform polar tropospheric warming in CPL simulations (Fig. 2a,b) but weakly surface-enhanced warming in SOM simulations (Supplementary Fig. 3a,b), suggesting a role for ocean dynamics in mediating the response. Importantly, the full tropospheric temperature responses to regional forcings also sum to the GLOBAL response in both SOM (Supplementary Fig. 3d,e) and CPL (Fig. 2d,e) simulations. Thus, the strong bottom-heavy warming profile (weakened temperature inversion) in polar regions under global forcing can be attributed primarily to POLAR forcing (annually and in winter and summer alone; Supplementary Fig. 4). The warming profiles seen in these simulations are slightly different from the pronounced mid-tropospheric Arctic warming peak seen in response to remote radiative forcing in idealized aquaplanet simulations that lack both sea ice and land[18].

In addition to TOA radiative forcing, the warming pattern can also be influenced by surface forcing due to ocean dynamics, which can act either through transient heat uptake or anomalous oceanic heat transport. In particular, anomalous poleward heat transport into the Arctic under global forcing has been suggested to play a role in Arctic amplification[15,23,24]. Since the radiative forcing structure is the

Table 1 | Arctic and Antarctic amplification of TAS

Experiment	$TAS_{30°S-30°N}$ (°C)	$TAS_{60°S-90°S}$ (°C)	$TAS_{60°N-90°N}$ (°C)	$\frac{TAS_{60°S-90°S}}{TAS_{30°S-30°N}}$	$\frac{TAS_{60°N-90°N}}{TAS_{30°S-30°N}}$	$TAS_{global\ mean}$ (°C)	$\frac{TAS_{global\ mean}}{R_{global\ mean}}$ (°C W^{-1} m^2)
GLOBAL-CPL	2.93	4.98	7.33	1.70	2.50	3.62	0.50
TROP-CPL	0.28	0.01	0.32	0.04	1.14	0.16	0.16
MLAT-CPL	2.17	2.51	3.07	1.16	1.42	2.42	0.46
POLAR-CPL	0.20	1.76	3.14	8.80	15.70	0.63	0.80

Amplification is defined as a ratio of warming averaged poleward of 60° N and 60° S, divided by the warming averaged over 30° S–30° N. *R* denotes the radiative forcing.

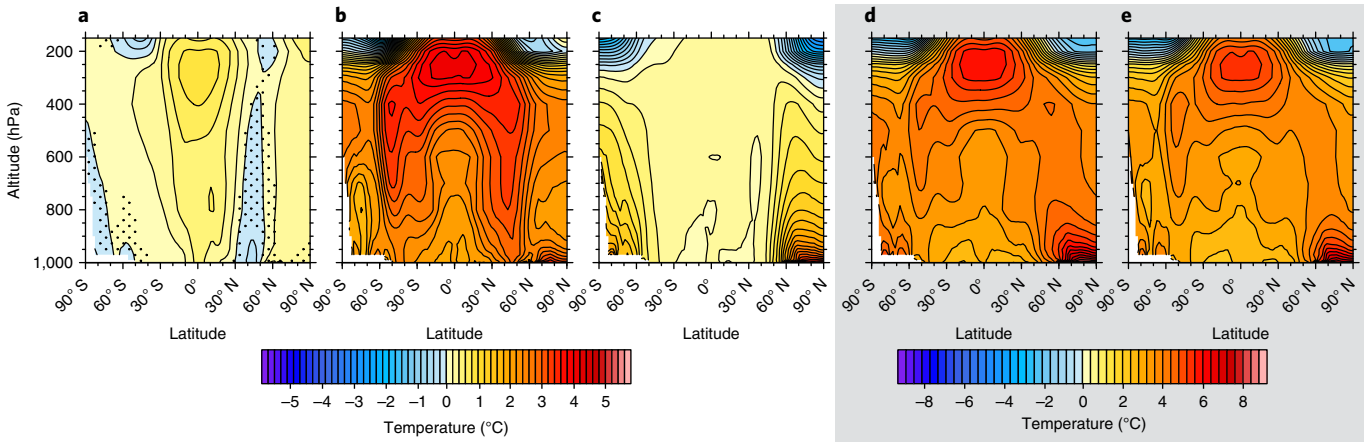

Fig. 2 | Tropospheric temperature responses. a–d, Tropospheric zonal mean, ensemble mean temperature responses for TROP-CPL (**a**), MLAT-CPL (**b**), POLAR-CPL (**c**) and GLOBAL-CPL (**d**). Ensemble mean values that are significantly different from zero at the 95% confidence level (using a two-tailed *t*-test) are non-stippled. **e**, Sum of the response of TROP-CPL, MLAT-CPL and POLAR-CPL. The grey shaded background highlights the similarity between the GLOBAL and sum responses.

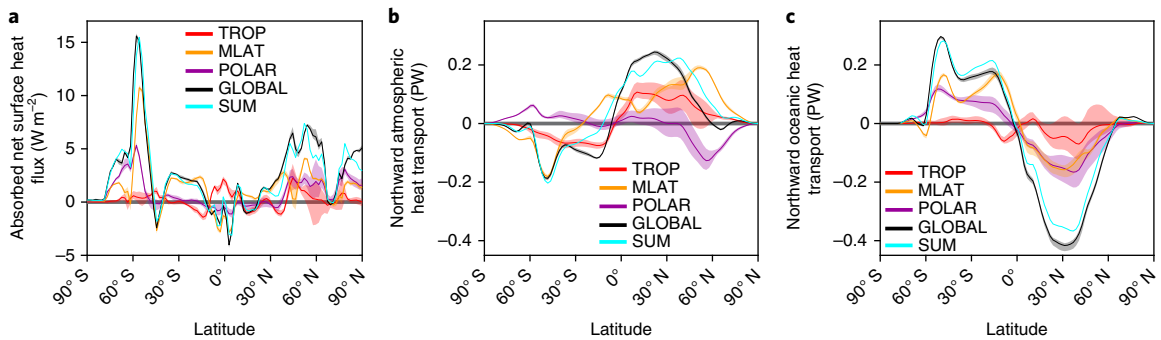

Fig. 3 | Heat uptake and transport by the ocean and atmosphere. Zonal mean climate response for TROP-CPL (red), MLAT-CPL (orange), POLAR-CPL (magenta) and GLOBAL-CPL (black). Shading indicates the ensemble range. The sum for the regional experiments is displayed in cyan. **a**, Absorbed net surface heat flux by the ocean. **b**,**c**, Northward heat transport response in the atmosphere (**b**) and ocean (**c**).

same in both CPL and SOM simulations, differences in responses can be attributed to ocean dynamics. Both heat uptake (Fig. 3a) and anomalous oceanic meridional heat transport (Fig. 3c) from the regional forcing simulations approximately sum to that of GLOBAL.

The polar warming in SOM simulations (Supplementary Fig. 1) is much larger than in CPL simulations (Fig. 1b), highlighting the importance of high-latitude ocean dynamics in damping surface warming, particularly in the Southern Hemisphere[24,25]. The strong heat uptake in the Southern Ocean and moderate heat uptake in the subpolar Northern Hemisphere is evident in MLAT and POLAR, where forcing coincides with the Southern Ocean, while TROP produces heat uptake within the tropical oceans (Fig. 3a).

The anomalous oceanic heat transport is generally equatorward in both hemispheres, most strongly for MLAT and POLAR; these changes reflect northward Ekman transport of heat taken up at the Southern Ocean surface[25] and a slowdown in the Atlantic Meridional Overturning Circulation[24]. Anomalous oceanic heat transport in the deep tropics is poleward in TROP, reflecting poleward transport of warmed surface waters by subtropical cells. Thus, transient ocean heat uptake is important for polar amplification, while the role of anomalous oceanic heat transport into the Arctic is small in our experiments and can primarily be attributed to midlatitude forcing.

Poleward atmospheric heat transport increases substantially everywhere in TROP and MLAT (Fig. 3b), but decreases slightly over

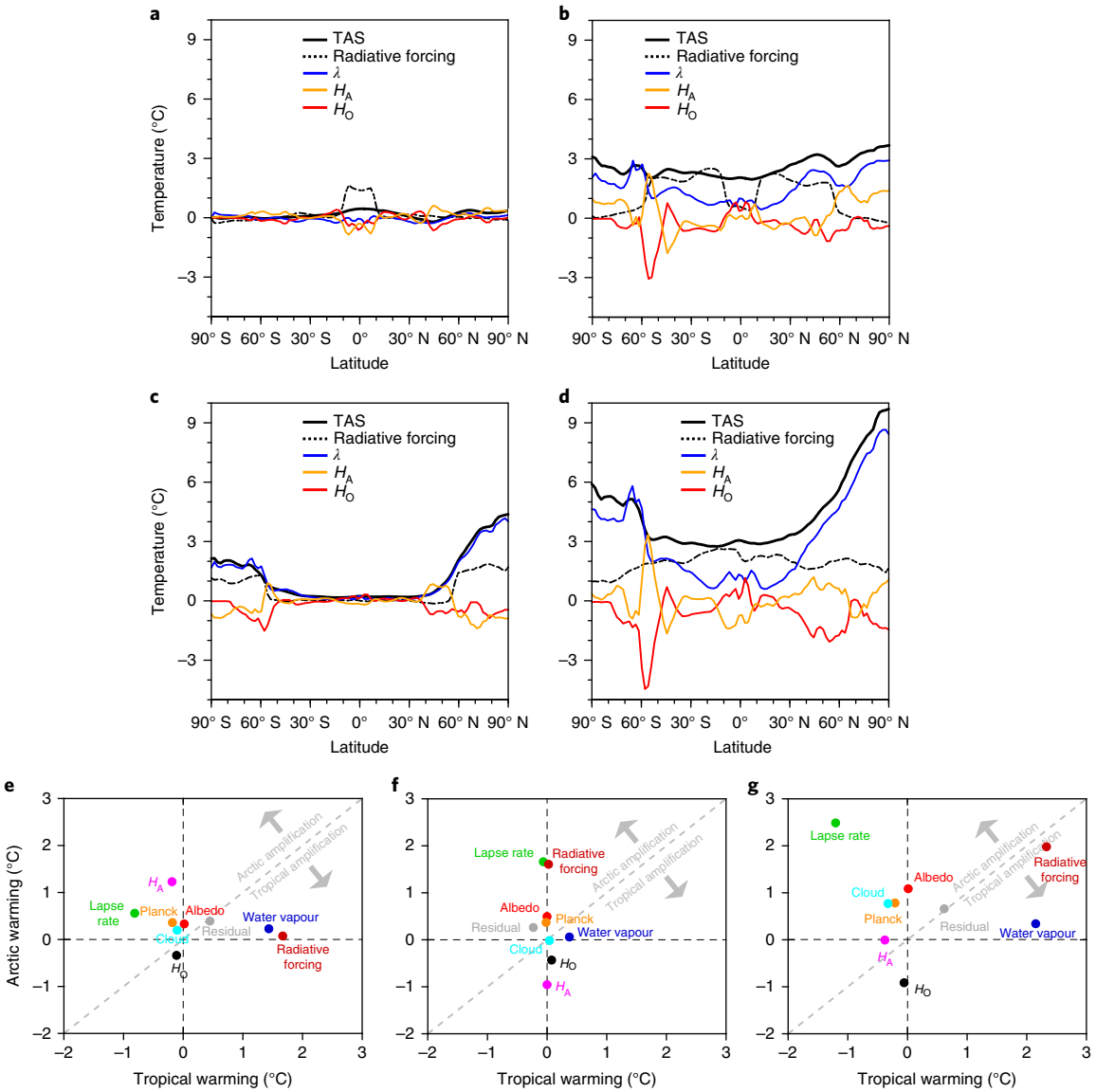

Fig. 4 | Warming contributions by different physical processes. a–d, Contributions of radiative forcing, oceanic heat uptake (H_O; the absorbed net surface heat flux), heat divergence due to atmospheric heat transport (H_A; calculated by the difference between TOA radiative imbalance and the absorbed net surface heat flux) and the local feedback parameter (λ) to the zonal mean TAS warming in TROP-CPL (**a**), MLAT-CPL (**b**), POLAR-CPL (**c**) and GLOBAL-CPL (**d**). **e–g**, Contributions of the individual feedbacks to warming in the broad tropics (30° S–30° N) and Arctic (60° N–90° N) in MLAT-CPL (**e**), POLAR-CPL (**f**) and GLOBAL-CPL (**g**). The uncertainty of the decomposition is indicated by the residual.

30° N–60° N and and 30° S–60° S in POLAR, consistent with expectations that the atmosphere will act to transport energy away from regions of radiative energy accumulation[22,26]. The result is relatively uniform patterns of surface warming in TROP and MLAT, but polar-amplified warming in POLAR. These findings are in good agreement with the results of diffusive moist energy balance models[22,26]: extra-polar forcing leads to increased poleward energy transport and a flat temperature response due to down-gradient transport of anomalous moist static energy, while polar forcing leads to large polar warming and little tropical warming, with a decrease in poleward atmospheric heat transport.

Next, we seek to quantify the contributions of individual processes to polar amplification, aided by the fact that the radiative forcings and climate responses (Figs 1–3) associated with forcing in each region sum approximately to the global response. First, we decompose the zonal mean temperature response into 'warming contributions' from radiative forcing, local feedback, atmospheric heat transport and net surface heat flux (ocean heat uptake) in the CPL simulations (Fig. 4a–d; see the Methods section 'Feedback calculation'). For deep-tropical forcing, the small amount of Arctic warming is entirely caused by atmospheric heat transport (orange line in Fig. 4a). In contrast, local feedbacks and atmospheric heat transport both contribute to Arctic warming in MLAT-CPL (blue and orange lines, respectively, in Fig. 4b). Meanwhile, local feedbacks dominate polar warming in POLAR-CPL (blue line in Fig. 4c), with local radiative forcing contributing to warming, and heat transport changes acting to cool the poles. While asymmetry between Antarctic and Arctic warming can be largely attributed to inter-hemispheric asymmetry in ocean heat uptake and atmospheric heat transport under midlatitude forcing, it is primarily due to asymmetry in local feedbacks under polar forcing.

Finally, we employ radiative kernels[27,28] to decompose Arctic amplification into contributions from individual local feedbacks[4,10] for the MLAT-CPL, POLAR-CPL and GLOBAL-CPL simulations

(Methods). This allows us to (1) quantify the importance of individual feedbacks and (2) test how sensitive this decomposition is to changes in the spatial pattern of the radiative forcing. Consistent with the results of Pithan and Mauritsen[4], we find that in the POLAR-CPL and GLOBAL-CPL experiments the largest contribution to Arctic amplification is the lapse-rate feedback, reflecting the bottom-heavy tropospheric warming profile seen in Fig. 2c,d; curvature in the Planck feedback (see Methods for the definition) and surface-albedo feedback each contribute to Arctic amplification, but are of secondary importance (Fig. 4f–g and Supplementary Fig. 5). However, the exact contribution of each type of feedback differs considerably depending on where forcing is applied. Moreover, atmospheric heat transport strongly contributes to Arctic amplification (of comparable magnitude to the lapse-rate feedback) in MLAT (Fig. 4e and Supplementary Fig. 5), but acts to decrease Arctic amplification in POLAR. These results highlight the limitations of interpreting causal mechanisms of Arctic amplification from GLOBAL alone. For instance, radiative forcing appears to contribute to tropically amplified warming under GLOBAL forcing (Fig. 4g), but when forcing is applied region by region, radiative forcing in polar regions is seen to be the primary driver of Arctic amplification (Figs. 1 and 4f). Thus, reducing radiative forcing at the pole may be a more effective policy to minimize Arctic amplification than previously thought.

The question of which processes contribute most to polar amplification is still strongly debated. Here, we have found that the response of the climate system to different regional forcing is remarkably linear, both in transient coupled atmosphere–ocean simulations and equilibrium slab ocean simulations. These results suggest that while remote forcing from outside the polar regions can contribute to polar warming, it makes a negligible contribution to polar amplification. Moreover, polar-amplified downwelling surface longwave radiation is largely due to POLAR forcing (Supplementary Fig. 6b). Thus, enhanced downwelling longwave radiation in polar regions should not necessarily be taken as evidence for remote forcing of polar amplification (see, for instance, the discussion in Lee et al.[29]). The reduction in Arctic downwelling surface shortwave radiation (mostly due to increases in polar cloudiness) can be about equally attributed to POLAR and MLAT forcing (Supplementary Fig. 6a). While MLAT forcing does not contribute to polar amplification, it does account for a substantial fraction of polar warming due to strong polar feedbacks that amplify the heat transport-induced warming (Fig. 4b).

Furthermore, we have identified the lapse-rate feedback as the dominant feedback contributing to Arctic amplification, with curvature in the Planck feedback, and the surface-albedo feedback playing smaller roles. This leads us to hypothesize that previous work highlighting the role of surface-albedo feedback[7] in Arctic amplification may have arrived at this conclusion due to prescribing SST and sea-ice boundary conditions instead of using a fully coupled modelling approach in which changes are initiated by CO_2 forcing. Indeed, the lapse-rate feedback itself is forcing dependent[30], suggesting that applying CO_2 forcing within a coupled model framework is needed to evaluate the system response. Because the relative contribution of each feedback and the role of meridional heat transport are strongly dependent on the spatial pattern of radiative forcing, the key mechanisms of polar amplification are difficult to evaluate within traditional simulations of CO_2 forcing applied globally.

We propose that the dynamical framework presented here can be generalized to study the influence of varying spatial radiative forcing patterns on other aspects of climate response. We emphasize that our analysis does not explore inter-model differences. However, given the robustness of the warming structure in response to idealized surface heat fluxes[22], it seems unlikely we would obtain qualitatively different responses with different models. Still, conducting similar experiments in other models would allow us to further increase our confidence in the relative importance and precise magnitude of the individual physical processes identified here.

Online content

Any methods, additional references, Nature Research reporting summaries, source data, statements of data availability and associated accession codes are available at https://doi.org/10.1038/s41558-018-0339-y.

Received: 17 June 2018; Accepted: 17 October 2018;
Published online: 19 November 2018

References

1. Manabe, S. & Wetherald, R. The effects of doubling the CO_2 concentrations on the climate of a general circulation model. *J. Atmos. Sci.* **32**, 3–15 (1975).
2. Holland, M. M. & Bitz, C. M. Polar amplification of climate change in coupled models. *Clim. Dynam.* **21**, 221–232 (2003).
3. Bintanja, R., Graversen, R. G. & Hazeleger, W. Arctic winter warming amplified by the thermal inversion and consequent low infrared cooling to space. *Nat. Geosci.* **4**, 758–761 (2011).
4. Pithan, F. & Mauritsen, T. Arctic amplification dominated by temperature feedbacks in contemporary climate models. *Nat. Geosci.* **7**, 181–184 (2014).
5. Park, K., Kang, S. M., Kim, D., Stuecker, M. F. & Jin, F.-F. Contrasting local and remote impacts of surface heating on polar warming and amplification. *J. Clim.* **31**, 3155–3166 (2018).
6. Screen, J. A. & Simmonds, I. The central role of diminishing sea ice in recent Arctic temperature amplification. *Nature* **464**, 1334–1337 (2010).
7. Screen, J. A., Deser, C. & Simmonds, I. Local and remote controls on observed Arctic warming. *Geophys. Res. Lett.* **39**, L10709 (2012).
8. Taylor, P. C. et al. A decomposition of feedback contributions to polar warming amplification. *J. Clim.* **26**, 7023–7043 (2013).
9. Winton, M. Amplified Arctic climate change: what does surface albedo feedback have to do with it? *Geophys. Res. Lett.* **33**, L03701 (2006).
10. Goosse, H. et al. Quantifying climate feedbacks in polar regions. *Nat. Commun.* **9**, 1919 (2018).
11. Graversen, R. G., Mauritsen, T., Tjernström, M., Källén, E. & Svensson, G. Vertical structure of recent Arctic warming. *Nature* **451**, 53–56 (2008).
12. Lu, J. & Cai, M. Quantifying contributions to polar warming amplification in an idealized coupled general circulation model. *Clim. Dynam.* **34**, 669–687 (2010).
13. Lee, S., Gong, T., Johnson, N., Feldstein, S. B. & Pollard, D. On the possible link between tropical convection and the Northern Hemisphere Arctic surface air temperature change between 1958 and 2001. *J. Clim.* **24**, 4350–4367 (2011).
14. Spielhagen, R. F. et al. Enhanced modern heat transfer to the Arctic by warm Atlantic water. *Science* **331**, 450–453 (2011).
15. Hwang, Y.-T., Frierson, D. M. W. & Kay, J. E. Coupling between Arctic feedbacks and changes in poleward energy transport. *Geophys. Res. Lett.* **38**, L17704 (2011).
16. Huang, Y., Xia, Y. & Tan, X. On the pattern of CO_2 radiative forcing and poleward energy transport. *J. Geophys. Res. Atmos.* **122**, 10578–10593 (2017).
17. Shindell, D. & Faluvegi, G. Climate response to regional radiative forcing during the twentieth century. *Nat. Geosci.* **2**, 294–300 (2009).
18. Kang, S. M., Park, K., Jin, F.-F. & Stuecker, M. F. Common warming pattern emerges irrespective of forcing location. *J. Adv. Model Earth Syst.* **9**, 2413–2424 (2017).
19. Woods, C. & Caballero, R. The role of moist intrusions in winter Arctic warming and sea ice decline. *J. Clim.* **29**, 4473–4485 (2016).
20. Alexeev, V. A., Langen, P. L. & Bates, J. R. Polar amplification of surface warming on an aquaplanet in 'ghost forcing' experiments without sea ice feedbacks. *Clim. Dynam.* **24**, 655–666 (2005).
21. Chung, C. E. & Räisänen, P. Origin of the Arctic warming in climate models. *Geophys. Res. Lett.* **38**, L21704 (2011).
22. Rose, B. E. J., Armour, K. C., Battisti, D. S., Feldl, N. & Koll, D. D. B.The dependence of transient climate sensitivity and radiative feedbacks on the spatial pattern of ocean heat uptake. *Geophys. Res. Lett.* **41**, 1071–1078 (2014).
23. Bitz, C. M., Gent, P. R., Woodgate, R. A., Holland, M. M. & Lindsay, R. The influence of sea ice on ocean heat uptake in response to increasing CO_2. *J. Clim.* **19**, 2437–2450 (2006).
24. Marshall, J. et al. The ocean's role in the transient response of climate to abrupt greenhouse gas forcing. *Clim. Dynam.* **44**, 2287–2299 (2015).
25. Armour, K. C., Marshall, J., Scott, J., Donohoe, A. & Newsom, E. R. Southern Ocean warming delayed by circumpolar upwelling and equatorward transport. *Nat. Geosci.* **9**, 549–554 (2016).
26. Roe, G. H., Feldl, N., Armour, K. C., Hwang, Y.-T. & Frierson, D. M. W. The remote impacts of climate feedbacks on regional climate predictability. *Nat. Geosci.* **8**, 135–139 (2015).

27. Shell, K. M., Kiehl, J. T. & Shields, C. A. Using the radiative kernel technique to calculate climate feedbacks in NCAR's community atmospheric model. *J. Clim.* **21**, 2269–2282 (2008).
28. Bitz, C. M. et al. Climate sensitivity of the community climate system model, version 4. *J. Clim.* **25**, 3053–3070 (2012).
29. Lee, S., Gong, T., Feldstein, S. B., Screen, J. A. & Simmonds, I. Revisiting the cause of the 1989–2009 Arctic surface warming using the surface energy budget: downward infrared radiation dominates the surface fluxes. *Geophys. Res. Lett.* **44**, 10654–10661 (2017).
30. Cronin, T. W. & Jansen, M. F. Analytic radiative-advective equilibrium as a model for high-latitude climate. *Geophys. Res. Lett.* **43**, 449–457 (2015).

Acknowledgements

M.F.S. was supported by the Institute for Basic Science (project code IBS-R028-D1) and NOAA Climate and Global Change Postdoctoral Fellowship Program, administered by UCAR's Cooperative Programs for the Advancement of Earth System Sciences. C.M.B. was supported by NOAA grant CPO NA115OAR4310161. C.P. was supported by a JISAO postdoctoral fellowship. K.C.A. and Y.D. were supported by NSF grants AGS-1752796 and OCE-1523641. S.M.K. and D.K. were supported by the Basic Science Research Program through the National Research Foundation of Korea, funded by the Ministry of Science, ICT and Future Planning (2016R1A1A3A04005520). S.M. was supported by the Australian Research Council (grant numbers FT160100162 and CE170100023). F.-F.J. was supported by NSF grant AGS-1813611 and Department of Energy grant DE-SC0005110. Computing resources were provided by the University of Southern California's Center for High-Performance Computing.

Author contributions

M.F.S. designed the study, conducted the model experiments and wrote the initial manuscript draft. M.F.S., C.M.B. and D.K. performed the analysis. All authors contributed to the interpretation of the results and improvement of the manuscript.

Competing interests

The authors declare no competing interests.

Additional information

Supplementary information is available for this paper at https://doi.org/10.1038/s41558-018-0339-y.

Reprints and permissions information is available at www.nature.com/reprints.

Correspondence and requests for materials should be addressed to M.F.S.

Publisher's note: Springer Nature remains neutral with regard to jurisdictional claims in published maps and institutional affiliations.

© The Author(s), under exclusive licence to Springer Nature Limited 2018

Methods

Model experiments. We used the Community Earth System Model version 1.2.2 (ref. [31]) with the finite volume Community Atmosphere Model version 4 (ref. [32]). Atmosphere and land have a nominally 2° horizontal resolution and ocean and sea ice have a nominally 1° horizontal resolution. A hierarchy of configurations was used with CO_2 concentrations prescribed either regionally (TROP, MLAT and POLAR) or globally (GLOBAL).

Fully coupled experiments with an active dynamical ocean model were initialized from year 901 of a fully coupled pre-industrial control simulation at a quasi-equilibrated ocean state. We branched off one control (CTRL-CPL) and ten ensemble members for the experiments with abruptly quadrupled CO_2 concentrations either in the deep tropics (TROP-CPL) or symmetrically in the polar regions of both hemispheres (POLAR-CPL). The high-latitude forcing area (POLAR) was defined to entirely cover the polar regions in both hemisphere to prevent pronounced asymmetric perturbations of the climate system[33]. The area over which the CO_2 forcing was applied in TROP and POLAR was approximately equal. Also, we conducted ensembles (each with five members) for two additional experiments forced with abruptly quadrupled CO_2 (1) symmetrically in the rest of the tropics, subtropics and midlatitudes (MLAT-CPL) and (2) globally (GLOBAL-CPL), respectively. These abrupt CO_2 quadrupling experiments can be used to infer the spatial climate response patterns to slowly varying forcing, as discussed in previous studies[34,35].

The forcing structure is displayed in Fig. 1a. Each ensemble member has a small perturbation in the initial atmospheric state. We used a 60-year average of CTRL-CPL (years 901–960) as the control reference climate for our coupled experiments. The perturbed climate in TROP-CPL, MLAT-CPL, POLAR-CPL and GLOBAL-CPL was calculated using 50-year averages of each ensemble member (years 911–960), calculating the anomalies of each ensemble member respective to CTRL-CPL, and then calculating the ensemble mean of these anomalies. The time averages are sufficiently long so that the ensemble spread is very small.

To show the robustness of our results, we show whenever possible the ensemble mean response together with the ensemble spread. A two-tailed *t*-test is employed in Fig. 2 and Supplementary Fig. 4 to test whether the ensemble mean response is significantly different from zero.

Second, we used the SST and sea-ice concentration climatology calculated from the 60-year average of the above CTRL-CPL to generate the boundary conditions for additional AGCM experiments. Again, we conducted a control (CTRL-AGCM) and four experiments (TROP-AGCM, MLAT-AGCM, POLAR-AGCM and GLOBAL-AGCM) with the same forcing structure (Fig. 1a). Each experiment was run for 80 years, and the last 70 years (911–980) were used to calculate a time average. The anomalies for these experiments are respective to CTRL-AGCM. The TOA radiative imbalance from these experiments was used to calculate the effective radiative forcing (R)[36], following the Radiative Forcing Model Intercomparison Project protocol[37], for each prescribed CO_2 pattern.

Third, we used the climatological Q fluxes[28] calculated from the 60-year average of the above CTRL-CPL for a series of SOM experiments. Integrating the slab ocean with these climatological Q fluxes leads to a very similar model climatology compared with the fully coupled run[28]. Again, we conducted a control (CTRL-SOM) and four experiments (TROP-SOM, MLAT-SOM, POLAR-SOM and GLOBAL-SOM) with the same forcing structure (Fig. 1a). Each experiment was run for 120 years and the last 90 years (931–1020) were used to calculate the time average. The anomalies for these experiments are respective to CTRL-SOM. The response in these experiments can be seen as the final equilibrated climate in contrast with the transient response in the fully coupled experiments. The surface temperature and sea-ice responses in the polar regions are much larger in the SOM experiments compared with the CPL experiments (especially for midlatitude and polar forcing), and thereby constitute a large climate state shift.

We show that the climate response is spatially very linear (that is, the response to local forcing sums approximately to the response to global forcing for various important variables) over sufficiently long timescales (50-year averages in CPL) and large enough spatial scales (that is, zonal and regional averages). We expect the system to be less linear at shorter timescales and/or smaller spatial scales[38].

Feedback calculation. We write the energy balance of an atmospheric column locally at each horizontal grid point (i, j) in the following form[22,39]:

$$H_{\mathrm{O}}^{i,j} = \lambda^{i,j}\mathrm{TAS}^{i,j} + R^{i,j} - H_{\mathrm{A}}^{i,j} \tag{1}$$

Using radiative kernels[27], which are defined as the change in TOA radiation due to a local change in climate variables such as TAS or specific humidity Q, we can further decompose the local feedback parameter $\lambda^{i,j}$. All anomaly fields in the feedback calculation are taken with respect to the CTRL-CPL simulation, and R is used in the calculation of cloud feedbacks[27]. The effective radiative forcing (as calculated via the standard Radiative Forcing Model Intercomparison Project protocol[37]) has small contributions from water vapour, temperature and cloud changes associated with land and sea-ice warming, which are sometimes considered fast feedback processes. Likewise, the feedback calculation includes very small contributions from tropospheric water vapour and temperature changes in the AGCM experiments that are sometimes considered part of the forcing. The individual feedback components are the Planck feedback (PL), albedo feedback (AL), lapse-rate feedback (LR), water vapour feedback (WV), shortwave cloud radiative effect (CSW) and longwave cloud radiative effect (CLW), and a residual ϵ:

$$\lambda^{i,j} = \lambda_{\mathrm{PL}}^{i,j} + \lambda_{\mathrm{AL}}^{i,j} + \lambda_{\mathrm{LR}}^{i,j} + \lambda_{\mathrm{WV}}^{i,j} + \lambda_{\mathrm{CSW}}^{i,j} + \lambda_{\mathrm{CLW}}^{i,j} + \epsilon \tag{2}$$

where the feedbacks are all normalized with respect to the zonal mean TAS response. The Planck feedback is then decomposed into a global mean component and its curvature, $\lambda_{\mathrm{PL}}^{j} = \bar{\lambda}_{\mathrm{PL}} + \lambda_{\mathrm{PL}}^{\prime j}$, where the global mean component is calculated from GLOBAL-CPL and has a value of $-3.5\,\mathrm{W\,m^{-2}\,K^{-1}}$. For simplicity, we combine longwave and shortwave cloud radiative effects in the figures. We combine and rearrange equations (1) and (2) and write the local TAS response for a given region as a sum of the processes (Fig. 4e–g)[4]:

$$\begin{aligned}\langle \mathrm{TAS} \rangle \;=\; & \frac{1}{-\bar{\lambda}_{\mathrm{PL}}}\left[\langle \lambda_{\mathrm{PL}}^{\prime j}\mathrm{TAS}^{j}\rangle + \langle \lambda_{\mathrm{AL}}^{j}\mathrm{TAS}^{j}\rangle\right] \\ & + \langle \lambda_{\mathrm{LR}}^{j}\mathrm{TAS}^{j}\rangle + \langle \lambda_{\mathrm{WV}}^{j}\mathrm{TAS}^{j}\rangle \\ & + \langle \lambda_{\mathrm{CSW}}^{j}\mathrm{TAS}^{j}\rangle + \langle \lambda_{\mathrm{CLW}}^{j}\mathrm{TAS}^{j}\rangle \\ & \left[-\langle H_{\mathrm{O}}^{j}\rangle + \langle R^{j}\rangle - \langle H_{\mathrm{A}}^{j}\rangle + \epsilon\right]\end{aligned} \tag{3}$$

The temperature contributions by each feedback in the bracket are obtained by multiplying the locally defined zonal mean (denoted by a superscript j) feedbacks, obtained from the radiative kernels[27], with the zonal mean TAS response (in the respective experiment), then averaging (<>) the product (1) in the broad tropics (30° S–30° N) and (2) in the Arctic region (60° N–90° N). This calculation is done for the ensemble mean of the MLAT-CPL, POLAR-CPL and GLOBAL-CPL experiments. By contrasting these experiments, we can quantify the remote effect of radiative forcing on the local feedbacks and polar amplification. We emphasize that the feedback calculation employed here[4] provides an annual mean perspective and that the relative importance of individual feedbacks differs strongly between different seasons. The kernel method employed here neglects non-local feedbacks (as in previous studies). However, this approach is justified as these non-local feedbacks are small for the MLAT-CPL, POLAR-CPL and GLOBAL-CPL experiments, given that the residual ϵ is small when calculating the contributions to local warming due to the combination of local feedbacks.

In contrast, the residual term is relatively large in TROP-CPL as (1) the mean state changes are large compared with the perturbation in this experiment and/or (2) non-local feedbacks become increasingly important. Thus, we only use the kernel decomposition for the other three experiments, while we diagnose and show the zonal mean temperature contributions due to the bulk local feedback parameter $\lambda'^{j} = \lambda^{j} - \bar{\lambda}_{\mathrm{PL}}$ for every experiment (Fig. 4a–d):

$$\mathrm{TAS}^{j} = \frac{1}{-\bar{\lambda}_{\mathrm{PL}}}\left[\lambda'^{j}\mathrm{TAS}^{j} - H_{\mathrm{O}}^{j} + R^{j} - H_{\mathrm{A}}^{j}\right] \tag{4}$$

Data availability

The model source code to reproduce these experiments can be obtained from http://www.cesm.ucar.edu/models/cesm1.2/ and the modifications to prescribe spatially varying CO_2 concentrations can be obtained from the corresponding author.

References

31. Gent, P. R. et al. The community climate system model version 4. *J. Clim.* **24**, 4973–4991 (2011).
32. Neale, R. B. et al. The mean climate of the community atmosphere model (CAM4) in forced SST and fully coupled experiments. *J. Clim.* **26**, 5150–5168 (2013).
33. Kang, S. M., Held, I. M., Frierson, D. M. W. & Zhao, M. The response of the ITCZ to extratropical thermal forcing: idealized slab-ocean experiments with a GCM. *J. Climate* **21**, 3521–3532 (2008).
34. Santer, B. D., Wigley, T. M. L., Schlesinger, M. E. & Mitchell, J. F. B. *Developing Climate Scenarios from Equilibrium GCM Results* Technical Report 47 (Max-Planck-Institut-für-Meteorologie, 1990).
35. Tebaldi, C. & Arblaster, J. M. Pattern scaling: its strengths and limitations, and an update on the latest model simulations. *Climatic Change* **122**, 459–471 (2014).
36. Hansen, J. et al. Efficacy of climate forcings. *J. Geophys. Res.* **110**, D18104 (2005).
37. Pincus, R., Forster, P. M. & Stevens, B. The Radiative Forcing Model Intercomparison Project (RFMIP): experimental protocol for CMIP6. *Geosci. Model Dev.* **9**, 3447–3460 (2016).
38. Good, P. et al. Nonlinear regional warming with increasing CO_2 concentrations. *Nat. Clim. Change* **5**, 138–142 (2015).
39. Armour, K. C., Bitz, C. M. & Roe, G. H. Time-varying climate sensitivity from regional feedbacks. *J. Clim.* **26**, 4518–4534 (2013).